

Constraints on the temperature of the intergalactic medium at $z = 8.4$ with 21-cm observations

Bradley Greig^{1*}, Andrei Mesinger¹ and Jonathan C. Pober²

¹*Scuola Normale Superiore, Piazza dei Cavalieri 7, I-56126 Pisa, Italy*

²*Physics Department, Brown University, Providence, RI 02912, USA*

9 November 2021

ABSTRACT

We compute robust lower limits on the spin temperature, T_S , of the $z = 8.4$ intergalactic medium (IGM), implied by the upper limits on the 21-cm power spectrum recently measured by PAPER-64. Unlike previous studies which used a single epoch of reionization (EoR) model, our approach samples a large parameter space of EoR models: the dominant uncertainty when estimating constraints on T_S . Allowing T_S to be a free parameter and marginalizing over EoR parameters in our Markov Chain Monte Carlo code 21CMC, we infer $T_S \geq 3$ K (corresponding approximately to 1σ) for a mean IGM neutral fraction of $\bar{x}_{\text{HI}} \gtrsim 0.1$. We further improve on these limits by folding-in additional EoR constraints based on: (i) the dark fraction in QSO spectra, which implies a strict upper limit of $\bar{x}_{\text{HI}}[z = 5.9] \leq 0.06 + 0.05 (1\sigma)$; and (ii) the electron scattering optical depth, $\tau_e = 0.066 \pm 0.016 (1\sigma)$ measured by the *Planck* satellite. By restricting the allowed EoR models, these additional observations tighten the approximate 1σ lower limits on the spin temperature to $T_S \geq 6$ K. Thus, even such preliminary 21-cm observations begin to rule out extreme scenarios such as ‘cold reionization’, implying at least some prior heating of the IGM. The analysis framework developed here can be applied to upcoming 21-cm observations, thereby providing unique insights into the sources which heated and subsequently reionized the very early Universe.

Key words: galaxies: high-redshift – intergalactic medium – cosmology: theory – dark ages, reionization, first stars – diffuse radiation – early Universe

1 INTRODUCTION

Radiation emitted from the first stars and galaxies marked the end of the cosmic dark ages. The UV ionizing photons from these first sources escape into the intergalactic medium (IGM), reionizing the pervasive neutral hydrogen fog, bringing about the final major baryonic phase change of the Universe. This epoch of reionization (EoR) is rich in information on the formation and evolution of structures in the early Universe, including the nature of the first stars and galaxies and their impact on the IGM (see e.g. Barkana & Loeb 2007; Loeb & Furlanetto 2013; Zaroubi 2013).

The most promising observational tool for probing the EoR physics is the redshifted 21-cm spin-flip transition of neutral hydrogen (see e.g. Gnedin & Ostriker 1997; Madau et al. 1997; Shaver et al. 1999; Tozzi et al. 2000; Gnedin & Shaver 2004; Furlanetto et al. 2006; Morales & Wyithe 2010; Pritchard & Loeb 2012). The signal is expressed as the offset of the 21-cm brightness temperature, $\delta T_b(\nu)$, relative to the

CMB temperature, T_γ (e.g. Furlanetto et al. 2006):

$$\delta T_b(\nu) \approx 27 x_{\text{HI}} (1 + \delta_{\text{nl}}) \left(\frac{H}{dv_r/dr + H} \right) \left(1 - \frac{T_\gamma}{T_S} \right) \times \left(\frac{1+z}{10} \frac{0.15}{\Omega_m h^2} \right)^{1/2} \left(\frac{\Omega_b h^2}{0.023} \right) \text{ mK}, \quad (1)$$

where x_{HI} is the neutral fraction, T_S is the gas spin temperature, $\delta_{\text{nl}}(\mathbf{x}, z)$ is the evolved (Eulerian) overdensity, $H(z)$ is the Hubble parameter, dv_r/dr is the gradient of the line-of-sight component of the velocity and all quantities are evaluated at redshift $z = \nu_0/\nu - 1$, where ν_0 is the 21-cm frequency. Thus, the 21-cm signal probes both the ionization and thermal state of the IGM, and indirectly also the galaxies which regulate them. Moreover, as it is a line transition, it promises a 3D view of the early Universe.

Tapping into this physical bounty requires sensitive radio interferometers. First generation experiments such as the Low Frequency Array (LOFAR; van Haarlem et al. 2013; Yatawatta et al. 2013)¹, the Murchison Wide Field Array

* E-mail: bradley.greig@sns.it

¹ <http://www.lofar.org/>

(MWA; Tingay et al. 2013)² and the Precision Array for Probing the Epoch of Reionization (PAPER; Parsons et al. 2010)³ seek the statistical characterization of the 21-cm signal through a power spectrum (PS) measurement. Though no detection has been forthcoming thus far, steady progress is being made. Presently, the tightest upper limits come from the 64-dipole PAPER array, which constrained the spherically averaged PS over $0.1 \lesssim k \lesssim 0.4 h/\text{Mpc}$ to be less than $\lesssim 500 \text{ mK}^2$. Tomographic maps will have to wait for second-generation instruments such as the Square Kilometre Array (SKA; Koopmans et al. 2015)⁴ and the Hydrogen Epoch of Reionization Array (HERA; Beardsley et al. 2015)⁵.

Even these preliminary observations begin to constrain the state of the early Universe. From equation (1), we see that, once the IGM spin temperature is much hotter than the CMB ($T_s \gg T_\gamma$), the maximum achievable contrast in the 21-cm signal is of order 10 mK, sourced by order unity fluctuations in the neutral fraction during patchy reionization. However, prior to IGM heating when the signal is still in absorption against the CMB, the achievable dynamic range is much larger. For example, the adiabatically cooling IGM can reach values of $\delta T_b \sim -200 \text{ mK}$.⁶ Although the spatial fluctuations in the IGM temperature source a strong 21-cm PS signal ($\sim 100\text{s of mK}^2$; e.g. Pritchard & Furlanetto 2007; Pacucci et al. 2014), an even stronger signal would arise during so-called cold reionization (Mesinger et al. 2013). If reionization proceeded in a very cold IGM, the resulting contrast between the cold neutral regions (with $\delta T_b \sim -100$ to -200 mK), and the ionized regions (with $\delta T_b \sim 0 \text{ mK}$) could drive the large-scale 21-cm power to values in excess of $\sim 1000\text{s of mK}^2$ (e.g. Parsons et al. 2014). Such models can already be ruled out by current data.

Parsons et al. (2014) were the first to investigate constraints on ‘cold reionization’ from upper limits on the $z = 7.7$ 21-cm PS using the 32 dipole PAPER array. Ali et al. (2015), using tighter upper limits on the 21-cm PS at $z = 8.4$ from an extended 64 element PAPER array, subsequently obtained improved limits of $T_s > 4 \text{ K}$. Both works only used a simple analytic expression for the 21-cm PS during the EoR. An improved analysis was performed in Pober et al. (2015), making use of the semi numerical code 21CMFAST⁷ (Mesinger & Furlanetto 2007; Mesinger et al. 2011) to simulate both the EoR and IGM heating by X-rays. These authors varied the X-ray efficiency of early galaxies, in order to coarsely sample the IGM spin temperature, obtaining lower limits of $T_s \geq 5 \text{ K}$ for neutral fractions between 10 and 85 per cent.

Importantly, in each of these studies, only a single EoR model was used. The large-scale morphology (distribution of cosmic H II patches) depends on the properties of the sources and sinks of ionizing photons. These can produce large vari-

ations in both the shape and amplitude of the 21-cm PS during the EoR, even at a fixed redshift and mean neutral fraction (e.g. fig. 2 of Greig & Mesinger 2015).

In order to explore the impact of the EoR morphology on the constraints from PAPER-64, we utilize the recently developed Monte Carlo Markov Chain (MCMC)-based EoR analysis tool 21CMMC⁸ (Greig & Mesinger 2015). Using this theoretical framework, we recover improved, robust lower limits on the IGM temperature by marginalising over EoR models. We then strengthen these limits, by including reionization priors from observations of the dark pixel statistics of high- z quasars (McGreer et al. 2015) and the electron scattering optical depth, τ_e (Planck Collaboration XIII 2015).

The remainder of this paper is organized as follows. In Section 2, we outline our analysis methodology, while in Section 3, we discuss our improved constraints on the IGM temperature. Finally, in Section 4, we finish with our closing remarks. Throughout this work, we adopt the standard set of Λ CDM cosmological parameters: $(\Omega_m, \Omega_\Lambda, \Omega_b, n, \sigma_8, H_0) = (0.27, 0.73, 0.046, 0.96, 0.82, 70 \text{ km s}^{-1} \text{ Mpc}^{-1})$, measured from *WMAP* (Bennett et al. 2013) which are consistent with the latest results from *Planck* (Planck Collaboration XVI 2014).

2 METHODOLOGY

In Greig & Mesinger (2015), we developed 21CMMC, an MCMC-based analysis tool enabling the exploration of the EoR astrophysical parameter space. To simulate the reionization epoch, we assume a relatively popular, three parameter model which can accommodate a large set of physically motivated EoR morphologies. In this section, we summarize the EoR model sampled within 21CMMC and the modifications required to model ‘cold reionization’, deferring the reader to Greig & Mesinger (2015) for more technical discussions.

2.1 Modelling reionization within 21CMMC

For a given EoR parameter set, we simulate the 21-cm signal using the semi numerical simulation code 21CMFAST. 21CMFAST employs approximate but efficient methods for modelling the 21-cm signal, and is accurate when compared to computationally expensive radiative transfer simulations on scales relevant to 21-cm interferometry, $\geq 1 \text{ Mpc}$ (Mesinger et al. 2011; Zahn et al. 2011). The speed and efficiency of 21CMFAST makes it well suited for MCMC sampling. Below we outline the basic components of the EoR simulation; readers interested in more details are encouraged to read Mesinger & Furlanetto (2007) and Mesinger et al. (2011).

21CMFAST produces 3D realizations of the IGM density, velocity, source and ionization fields. A cubic volume of the linear density field is evolved using the Zel’dovich approximation (Zel’dovich 1970). The ionization fields are estimated using the excursion-set formalism outlined in Furlanetto et al. (2004), but modified to operate on the evolved

² <http://www.mwatelescope.org/>

³ <http://eor.berkeley.edu/>

⁴ <https://www.skatelescope.org>

⁵ <http://reionization.org>

⁶ This signal is achieved if the spin temperature is efficiently coupled to the gas kinetic temperature, through the Wouthuysen-Field mechanism (Wouthuysen 1952; Field 1958). Simple scaling relations (e.g. Furlanetto 2006; McQuinn 2012) show that this condition should be satisfied well before the IGM heating epoch.

⁷ <http://homepage.sns.it/mesinger/Sim>

⁸ <http://homepage.sns.it/mesinger/21CMMC.html>

density field (Mesinger et al. 2011). Following this prescription, the time-integrated number of ionizing photons are compared to the number of baryons within spherical regions of decreasing radius, R . A cell within the simulation volume is then classified as fully ionized if,

$$\zeta f_{\text{coll}}(\mathbf{x}, z, R, \bar{M}_{\text{min}}) \geq 1, \quad (2)$$

where ζ is the ionization efficiency which describes the conversion of mass into ionizing photons (see Section 2.1.1) and $f_{\text{coll}}(\mathbf{x}, z, R, \bar{M}_{\text{min}})$ is the fraction of collapsed matter within a spherical radius R residing within haloes larger than \bar{M}_{min} (Press & Schechter 1974; Bond et al. 1991; Lacey & Cole 1993; Sheth & Tormen 1999). Any cells not fully ionized (partial ionizations) are smoothed by the minimum smoothing scale of the cell, R_{cell} , and their ionization fraction from internal sources is set to $\zeta f_{\text{coll}}(\mathbf{x}, z, R_{\text{cell}}, \bar{M}_{\text{min}})$.

In this work, we adopt a popular three parameter model to characterize the EoR: (i) the ionizing efficiency of high- z galaxies; (ii) the mean free path of ionizing photons; (iii) the minimum virial temperature hosting star-forming galaxies. These EoR parameters are somewhat simplistic as they in effect average over redshift and/or halo mass dependences. However, this simple model suffices to describe a broad range of EoR morphologies, while at the same time providing a straightforward physical interpretation. In addition to these EoR parameters, here we include an additional free parameter: the mean IGM spin temperature. To help gain some intuition, below we summarize these four parameters, highlighting how they affect the 21-cm signal.

2.1.1 Ionizing efficiency, ζ

The ionizing efficiency of high- z galaxies (equation 2) can be expressed as

$$\zeta = 30 \left(\frac{f_{\text{esc}}}{0.2} \right) \left(\frac{f_{\star}}{0.05} \right) \left(\frac{N_{\gamma}}{4400} \right) \left(\frac{1.5}{1 + n_{\text{rec}}} \right) \quad (3)$$

where, f_{esc} is the fraction of ionizing photons escaping into the IGM, f_{\star} is the fraction of galactic gas in stars, N_{γ} is the number of ionizing photons produced per baryon in stars and n_{rec} is the average number of recombinations per baryon in the IGM.

The parameter ζ mainly serves to speed up/slow down reionization. Within this work, we take a flat prior over the range $\zeta \in [5, 200]$, which results in a range of reionization histories which are in broad agreement with current EoR constraints (Greig & Mesinger, in prep).

2.1.2 Minimum virial temperature of star-forming haloes, $T_{\text{vir}}^{\text{min}}$

The minimum threshold for a halo hosting a star-forming galaxy, regulating processes important for star formation such as gas accretion, cooling and retainment of supernovae outflows, can be defined in terms of its virial temperature, $T_{\text{vir}}^{\text{min}}$, which is related to its halo mass via, (e.g. Barkana & Loeb 2001)

$$M_{\text{min}} = 10^8 h^{-1} \left(\frac{\mu}{0.6} \right)^{-3/2} \left(\frac{\Omega_{\text{m}}}{\Omega_{\text{m}}^z} \frac{\Delta_{\text{c}}}{18\pi^2} \right)^{-1/2} \times \left(\frac{T_{\text{vir}}}{1.98 \times 10^4 \text{ K}} \right)^{3/2} \left(\frac{1+z}{10} \right)^{-3/2} M_{\odot}, \quad (4)$$

where μ is the mean molecular weight, $\Omega_{\text{m}}^z = \Omega_{\text{m}}(1+z)^3 / [\Omega_{\text{m}}(1+z)^3 + \Omega_{\Lambda}]$, and $\Delta_{\text{c}} = 18\pi^2 + 82d - 39d^2$ where $d = \Omega_{\text{m}}^z - 1$. The value $T_{\text{vir}}^{\text{min}} \approx 10^4$ K corresponds to the minimum temperature for efficient atomic cooling; however, efficient star formation likely requires more massive haloes, which are able to better retain and reincorporate supernovae driven outflows (e.g. Springel & Hernquist 2003).

The parameter $T_{\text{vir}}^{\text{min}}$ affects (i) when (at what redshift) reionization occurs, and (ii) the bias of the galaxies which are responsible. A higher value of $T_{\text{vir}}^{\text{min}}$ means that reionization happened later, with more large-scale ionization structure (at a fixed value of the mean neutral fraction; e.g. McQuinn et al. 2007). Here we assume a flat prior over the log of the virial temperature, within the range $T_{\text{vir}}^{\text{min}} \in [10^4, 5 \times 10^5]$ K. The lower limit corresponds to the atomic cooling threshold and the upper limit is roughly consistent with the host haloes of observed Lyman break galaxies at $z \sim 6-8$ (e.g. Kuhlen & Faucher-Giguère 2012; Barone-Nugent et al. 2014).

2.1.3 Mean free path of ionizing photons within ionized regions, R_{mfp}

The physical scales on which escaping ionizing photons are able to penetrate into the surrounding IGM depends strongly on both the number and properties of the absorption systems (such as Lyman limit and more diffuse systems). Typically below the resolution limits of EoR simulations, these systems behave as photon sinks, resulting in a maximum physical scale on which H II regions are capable of growing around the ionizing galaxies. The impact of photons sinks can be crudely interpreted as a maximum horizon for the ionizing photons, which can correspond to the maximum filtering scale in excursion-set EoR models. We denote this scale as R_{mfp} , noting that it depends on the time-integrated value of the mean free path through the ionized IGM during the EoR (Sobacchi & Mesinger 2014).

The parameter R_{mfp} most strongly impacts the large-scale ionization structure, with the large-scale 21-cm power dropping with decreasing R_{mfp} . Here, we adopt a flat prior over the range $R_{\text{mfp}} \in [5, 40]$ cMpc, motivated by sub-grid models of inhomogeneous recombinations (Sobacchi & Mesinger 2014), as well analytic estimates (Furlanetto & Oh 2005) and hydrodynamical simulations of the IGM (McQuinn et al. 2011; Emberson et al. 2013).

2.1.4 Mean IGM spin temperature, T_{S}

In order to recover limits on the ‘cold reionization’ model, in this work, we adopt a global value for the IGM spin temperature of the neutral cosmic gas during the EoR. This is an oversimplification, as we would expect spatial fluctuations in T_{S} sourced by the clustering of X-ray sources and the corresponding mean free path of the X-rays. However, in the relevant regime when the signal is the strongest (advanced stages of reionization with weak X-ray heating), a uniform T_{S} is a good approximation for most of the IGM as the hottest parts of the IGM which normally source large spatial fluctuations in T_{S} have already been ionized. The remaining neutral gas is distant from galaxies and its heating is governed by the harder X-rays with longer mean free

paths. This picture was quantitatively confirmed by Pober et al. (2015), who note that ignoring the spatial fluctuations in the spin temperature of the neutral IGM only impacts the large-scale 21-cm power during ‘cold reionization’ at the level of ~ 10 per cent (compared with the factor of 10 dependence of the large-scale power on the EoR morphology; e.g. fig. 2 in Greig & Mesinger 2015).

Within this work we explore the range $T_S \in [1.9, 30]$ K. This range encompasses the low IGM temperatures required to source a 21-cm signal strong enough to be ruled out by the upper limits in Ali et al. (2015). For reference, the IGM temperature in the absence of heating by astrophysical structures at $z = 8.4$ corresponds to 1.9 K (RECFAST; Seager et al. 1999, 2000), whereas the CMB temperature at that redshift is 25.6 K.

2.2 Computing the likelihood with 21CMMC

The principal data used for this analysis are the PS measurements from PAPER-64 presented in Ali et al. (2015). Here, we summarize the significant properties of their analysis; referring the reader to their work for detailed discussions of the observations and data reduction. Ali et al. (2015) analysed the complete observational campaign conducted with a 64-element PAPER array in South Africa over the span of 135 days from 2012 November to 2013 March. Their analysis focused on a 10 MHz frequency band centred on 151.5 MHz, corresponding to a 21-cm redshift of $z = 8.4$. The end result is a quoted upper limit on the 21-cm PS of $(22.4 \text{ mK})^2$ over the range of $0.15 < k < 0.5 \text{ h/Mpc}$, nearly a factor of four lower (in mK^2) than the previous best upper limit of Parsons et al. (2014). Approximately half of this increased sensitivity comes from a doubling of the number of antennas (64 elements, as opposed to the 32 used in the Parsons et al. 2014 analysis). The other half stems from an updated analysis method, with the principal three advances coming from improved redundant calibration using the methods of Zheng et al. (2014), fringe rate filtering (Parsons et al. 2015), and optimal quadratic estimators (Liu & Tegmark 2011; Trott et al. 2012; Dillon et al. 2013; Liu et al. 2014a,b).

The final PS measurements of Ali et al. (2015) correspond to nine data points spanning the range $0.1 < k < 0.5 \text{ h/Mpc}$, and their corresponding 2σ errors were obtained from a bootstrapping analysis. Within this work, we consider only data points with 2σ errors that are consistent with a null detection, as systematic errors remain in the data and will lead to significant excesses of power. Indeed within Ali et al. (2015), the ‘detections’ at low k are reported as likely being a result of foregrounds, whereas for the other ‘detections’ the causes are less certain. As a result, we are left with a total of four useable data points, which we can set as upper limits on the shape and amplitude of the 21-cm PS.

In the introductory paper of Greig & Mesinger (2015), we performed a maximum likelihood sampling of the EoR parameter space using a χ^2 statistic. To incorporate only the upper limits on the 21-cm PS, we retain the χ^2 statistic, however, we modify the likelihood computation. If the amplitude of the model PS falls below the observed value, we set our χ^2 to zero, resulting in equal likelihoods for the corresponding EoR parameters. If instead the model amplitude is above the observation, we compute the standard χ^2 , using the bootstrapped errors from Ali et al. (2015). Such an ap-

proach ensures we appropriately down weight EoR models producing amplitudes brighter than the PAPER-64 limits, while accepting all models fainter⁹.

Finally, we remove the conservative 25 per cent modelling uncertainty adopted in Greig & Mesinger (2015) when simulating the PS from 21CMFAST. This source of error is negligible when compared with the high upper limits on the 21-cm PS. Furthermore, we remove our conservative k -mode cut at $k = 0.15 \text{ Mpc}^{-1}$, which was included to remove Fourier modes contaminated by foregrounds, since this was already accounted for in the PAPER-64 limits.

2.3 Including observational priors on the EoR

In an effort to further improve the constraints on the IGM temperature, we consider two observational priors. First, we consider the strongest available constraints on the tail of the reionization epoch through measurements of the dark-pixel fraction of high- z quasars (McGreer et al. 2015). This approach provides model independent constraints on the IGM neutral fraction at $z = 5.9$ of $\bar{x}_{\text{HI}} \leq 0.06 + 0.05 (1\sigma)$, indicative of a completely (or almost nearly) reionized Universe by $z \approx 6$.

Secondly, we consider the measurement of the electron scattering optical depth to the CMB, $\tau_e = 0.066 \pm 0.016 (1\sigma)$ (Planck Collaboration XIII 2015). This corresponds to an instantaneous reionization redshift of $z_{\text{re}} = 8.8_{-1.4}^{+1.7}$, close to the observational redshift of the PAPER-64 21-cm PS constraints ($z = 8.4$).

These priors are incorporated into 21CMMC by computing the 21-cm PS at five different epochs, $z = 6, 7, 8.4, 10$ and 11 for each EoR model parameter set in the MCMC, whereas our χ^2 estimate is only performed at $z = 8.4$. We confirm that this sampling of the reionization history ensures we obtain accurate estimates for τ_e .

3 RESULTS

3.1 Constraints only from PAPER-64

In the top-left panel of Fig. 1, we report the joint 2D likelihood constraints of the IGM temperature and the IGM neutral fraction recovered from 21CMMC. To model the probability surface, we assume a normalized Gaussian distribution whereby each point in the T_S - \bar{x}_{HI} plane is assigned the probability, $P(\bar{x}_{\text{HI}}, T_S) \propto \exp(-\frac{1}{2}\chi^2)$, where the χ^2 value is determined by 21CMMC. In order to obtain this parameter surface, we marginalise over our three morphological EoR parameters (ζ , R_{mfp} and $T_{\text{vir}}^{\text{min}}$) assuming flat (uniform) priors for each across their allowed astrophysical values (see

⁹ This approach differs to that adopted by Pober et al. (2015). These authors use all data points as an upper limit, not just those consistent with zero. For each k -mode, they then compute the probability of obtaining their model 21-cm PS relative to the observation, and construct the likelihood by determining the joint probability of obtaining all data points for the model 21-cm PS. In doing so, these authors allow slightly higher amplitude 21-cm PS models than our approach; however, the relative differences between the two approaches should be minimal.

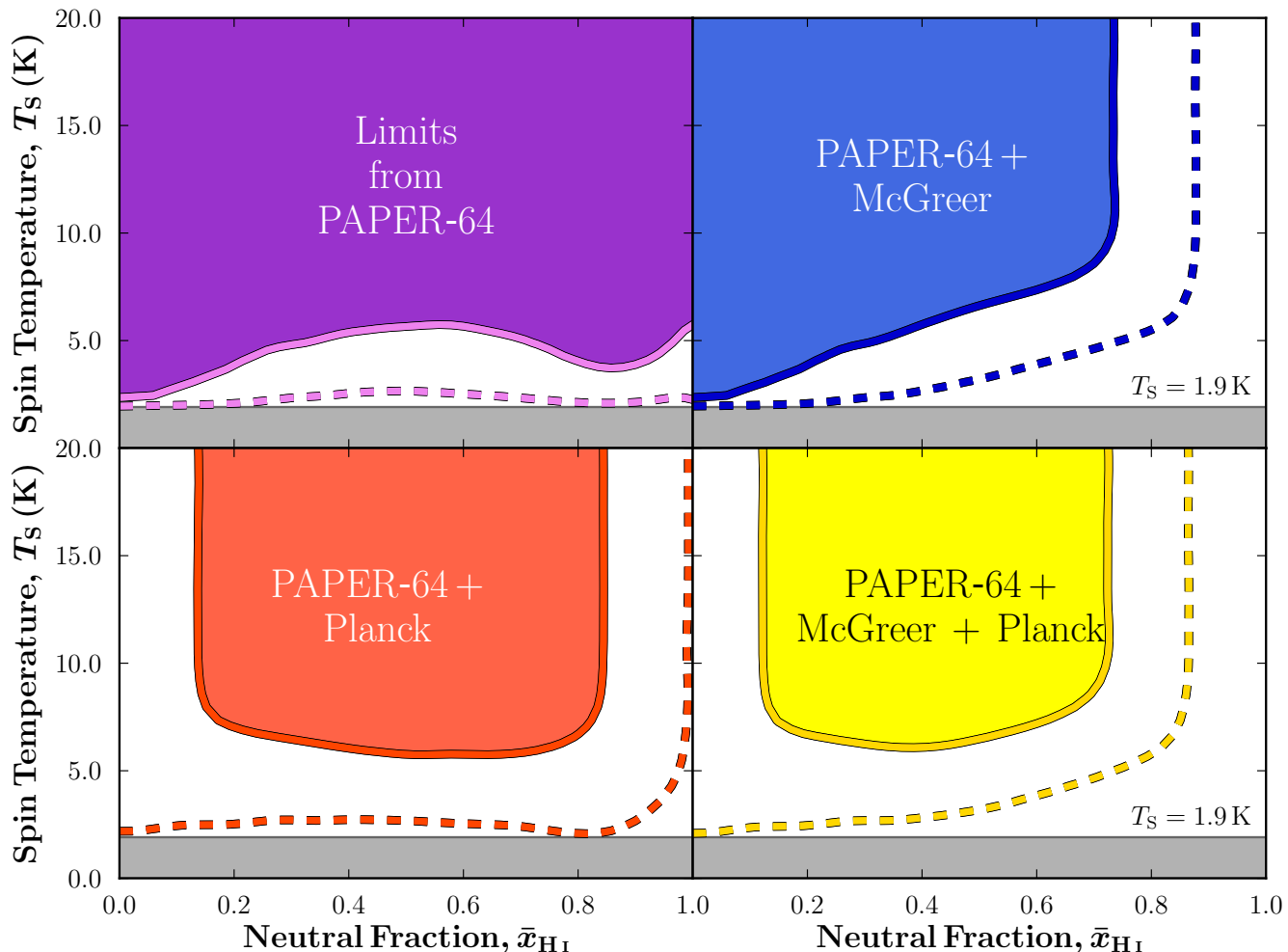


Figure 1. Joint 2D likelihood surfaces for the IGM spin temperature, T_S and the IGM neutral fraction, \bar{x}_{HI} , marginalised over our three morphological EoR parameters (ζ , R_{mfp} and $T_{\text{vir}}^{\text{min}}$) assuming flat (uniform) priors. Shaded regions correspond to $P(\bar{x}_{\text{HI}}, T_S) \geq 0.6$ (approximating 1σ), while dashed lines correspond to $P \geq 0.15$ (approximating 2σ). In the top-left panel, we provide the lower limits obtained from only the PAPER-64 constraints on the 21-cm PS. Top right, we include a prior on the IGM neutral fraction at $z = 5.9$ ($\bar{x}_{\text{HI}} \leq 0.06 + 0.05$, McGreer et al. 2015) to the PAPER-64 data. Bottom left, the inclusion of a prior on the electron scattering optical depth, τ_e ($\tau_e = 0.066 \pm 0.016$, Planck Collaboration XIII 2015). Bottom right, our tightest constraints on the IGM temperature, including both the $\bar{x}_{\text{HI}}[z = 5.9]$ and τ_e constraints. In all panels, the grey shaded region represents the lower limit on the IGM temperature in the absence of heating by astrophysical structures, $T_S = 1.9$ K.

Section 2.1). In all panels of Fig. 1, the shaded regions correspond to likelihoods of $P(\bar{x}_{\text{HI}}, T_S) \geq 0.6$; we consider the regions in white, corresponding to $P(\bar{x}_{\text{HI}}, T_S) \leq 0.6$, to be disfavoured by the data¹⁰

From the top-right panel, we see that the current PAPER-64 limits constrain the IGM temperature to be $T_S \gtrsim 5$ K at greater than 60 per cent confidence, for an

¹⁰ Since the observation only consists of an upper limit on the 21-cm PS, the values of $T_S \rightarrow \infty$ are allowed with relatively equal likelihood (see equation 1). Therefore, constructing standard confidence limits on T_S (defined to enclose a fixed area of the probability density function) is sensitive to the chosen range of the T_S priors. We instead choose to present our results as contours of equal likelihood, which are well defined, although the exact choice of the threshold value is arbitrary. The fiducial choice of $P \geq 0.6$ is loosely motivated by the probability of a normalized Gaussian distribution at 1σ . For illustrative purposes, in all panels in Fig 1, we additionally highlight an adopted threshold of $P \geq 0.15$ corresponding to the probability of a normalized Gaussian at 2σ .

IGM neutral fraction between 30 and 65 per cent. These reduce to $T_S \gtrsim 3$ K for a broader range in the IGM neutral fraction of $\bar{x}_{\text{HI}} \gtrsim 10$ per cent.

Qualitatively, the shape of the allowed T_S - \bar{x}_{HI} parameter space is almost identical to that presented in Pober et al. (2015). As discussed in that paper, this shape arises from the fact that the spin temperature term in equation (1) can roughly act as a multiplicative factor of the 21-cm PS during the EoR under the usual $T_S \gg T_\gamma$ assumption. This PS peaks during the midpoint of reionization, and in that regime the IGM does not need to be as cold to exceed the Ali et al. (2015) upper limits.

Quantitatively however, our lower limits on the IGM spin temperature are reduced by at least a factor of two compared to those in Pober et al. (2015). It is difficult to pin down all causes for this discrepancy, owing to the aforementioned different approaches in constructing the likelihood. Nevertheless, a relaxed lower limit is consistent with our naive expectations. The single EoR model used in Pober

et al. (2015) results in sizeable ionization structure on large scales. On the other hand, our EoR parameter space additionally includes models with substantially less large-scale ionization structure (compared at a fixed neutral fraction; see fig. 2 in Greig & Mesinger 2015), mostly sourced by smaller mean free paths of ionizing photons (e.g. Sobacchi & Mesinger 2014). Therefore, by marginalizing over all EoR models within our MCMC framework, we would expect a loosening of the lower limits owing to the broadening of the recovered probability distribution for the IGM temperature.

3.2 Constraints including additional EoR priors

In the second panel of Fig. 1, we include constraints on the end of reionization at $z \approx 6$ from McGreer et al. (2015). We find this drastically reduces the allowed parameter space, disfavouring models with $\bar{x}_{\text{HI}} > 0.75$. This behaviour is straightforward to interpret. To produce a ~ 10 per cent neutral IGM by $z \approx 6$ it would be very difficult to have a large \bar{x}_{HI} at $z = 8.4$, requiring unphysically-rapid reionization histories.

Next, we consider the inclusion of the τ_e prior from *Planck*, shown in the bottom-left panel of Fig. 1. The *Planck* measurement favours a midpoint of reionization close to the same redshift as the PAPER-64 measurement (albeit with broad error bars). This disfavors models with either too low or too high a neutral fraction, which are precisely those in which the signal is least sensitive to T_{S} . Thus our lower limits on T_{S} improve with respect to the top panels.

Finally, in the bottom right panel, we provide our lower limits combining both observational priors. Owing to the complimentary nature of the two priors, as discussed above, we now recover our most stringent lower limits on the IGM temperature of $T_{\text{S}} \gtrsim 6$. Even with a lower limits of $T_{\text{S}} \approx 6$ K, we can begin to place constraints on reionization scenarios such as ‘cold reionization’. As this temperature is above that of the IGM in the absence of heating by astrophysical structures (1.9 K), this implies that the IGM must have undergone some level of heating, ruling out a truly ‘cold’ (unheated) IGM. However, the relatively small amount of heating required does not yet begin to strongly constrain the physical processes that could be responsible (e.g. Pacucci et al. 2014).

Nevertheless, this approach highlights the utility of current 21-cm experiments. As more data are acquired, with better characterized systematics, these upper limits on the 21-cm PS amplitude should reduce, tightening the lower limits on the IGM temperature. Alternately, should a high 21-cm PS actually be detected, the implied lack of X-ray heating would have significant consequences for the star formation physics of the first galaxies.

4 CONCLUSION

One of the major astrophysical goals for the forthcoming decade is the statistical measurement of the 21-cm PS from the EoR. In probing the phase change from a neutral to ionized IGM, the EoR will yield rich information on the formation, growth and evolution of the first stars and galaxies and their influence on the IGM. For this reason several, dedicated first-generation radio instruments have been constructed, to

be followed by a wave of second-generation experiments with significantly larger collecting areas and sensitivity.

Although these experiments have yet to provide a detection, even current upper limits on the amplitude of the 21-cm PS can begin to constrain the physics of the EoR. In the absence of X-ray heating (or any other heating mechanism), the neutral IGM should remain ‘cold’, well below the CMB temperature. If reionization proceeds in such a cold IGM, the resulting contrast between cosmic ionized patches (with $\delta T_{\text{b}} \sim 0$ mK) and the cold, neutral patches (with $\delta T_{\text{b}} \sim -100$ mK) would drive the 21-cm signal to values in excess of current upper limits. Recently, both Ali et al. (2015) and Pober et al. (2015) used this fact to place limits on the IGM temperature during reionization, based on the 21-cm PS upper limits with PAPER-64.

In this work, we improve upon these existing analyses in several ways. Using a modified version of the MCMC-based EoR analysis tool 21CMMC (Greig & Mesinger 2015) we better sample the allowed astrophysical parameter space, improving on the fixed grid approach of Pober et al. (2015) and the analytic ‘toy’ model of Ali et al. (2015). This is achieved by allowing the mean IGM spin temperature, T_{S} to be a free parameter rather than varying the X-ray efficiency to recover a mean T_{S} as in Pober et al. (2015). Most importantly, by employing 21CMMC, we marginalize over a broad range of EoR models and morphologies. Both previous analyses assumed a single EoR model, thereby neglecting the fact that the EoR morphology can impact the amplitude of the 21-cm PS by up to an order of magnitude at a fixed neutral fraction (e.g. Greig & Mesinger 2015).

From the PAPER-64 upper limits alone, we can recover lower limits on the IGM temperature at $z = 8.4$ of $T_{\text{S}} \gtrsim 5$ K at greater than 60 per cent confidence for an IGM neutral fraction between $30 < \bar{x}_{\text{HI}} < 65$ per cent, which reduces to $T_{\text{S}} \gtrsim 3$ K when $\bar{x}_{\text{HI}} > 10$ per cent. We further tighten these constraints by including EoR priors. Folding-in priors on the tail end of the reionization epoch ($\bar{x}_{\text{HI}} \leq 0.06 + 0.05$ at $z = 5.9$; McGreer et al. 2015), as well as the integral constraint of $\tau_e = 0.066 \pm 0.016$ (Planck Collaboration XIII 2015), we obtain lower limits of $T_{\text{S}} \gtrsim 6$ K at greater than 60 per cent confidence. While not completely ruling out ‘cold reionization’ models, our results confirm that at least some level of prior IGM heating occurred. As both the quality and volume of available 21-cm data continues to increase, our framework will be able to provide unique insights into the high-energy processes inside the first galaxies.

ACKNOWLEDGEMENTS

This project has received funding from the European Research Council (ERC) under the European Union’s Horizon 2020 research and innovation programme (grant agreement No 638809 – AIDA). J.C.P. is supported by an NSF Astronomy and Astrophysics Fellowship under award AST-1302774.

REFERENCES

- Ali Z. S., et al., 2015, *ApJ*, 809, 61
- Barkana R., Loeb A., 2001, *Phys. Rep.*, 349, 125

- , 2007, *Rep. Prog. Phys.*, 70, 627
- Barone-Nugent R. L., et al., 2014, *ApJ*, 793, 17
- Beardsley A., Morales M., Lidz A., Malloy M., Sutter P., 2015, *ApJ*, 800, 128
- Bennett C. L., et al., 2013, *ApJS*, 208, 20
- Bond J. R., Cole S., Efstathiou G., Kaiser N., 1991, *ApJ*, 379, 440
- Dillon J. S., Liu A., Tegmark M., 2013, *Phys. Rev. D*, 87, 043005
- Emberson J. D., Thomas R. M., Alvarez M. A., 2013, *ApJ*, 763, 146
- Field G. B., 1958, *Proc. Inst. Radio Eng.*, 46, 240
- Furlanetto S. R., 2006, *MNRAS*, 371, 867
- Furlanetto S. R., Oh S. P., 2005, *MNRAS*, 363, 1031
- Furlanetto S. R., Oh S. P., Briggs F. H., 2006, *Phys. Rep.*, 433, 181
- Furlanetto S. R., Zaldarriaga M., Hernquist L., 2004, *ApJ*, 613, 1
- Gnedin N. Y., Ostriker J. P., 1997, *ApJ*, 486, 581
- Gnedin N. Y., Shaver P. A., 2004, *ApJ*, 608, 611
- Greig B., Mesinger A., 2015, *MNRAS*, 449, 4246
- Koopmans L. V. E., et al., 2015, in *Proc. Advancing Astrophys. Square Kilometre Array*
- Kuhlen M., Faucher-Giguère C.-A., 2012, *Monthly Notices of the Royal Astronomical Society*, 423, 862
- Lacey C., Cole S., 1993, *MNRAS*, 262, 627
- Liu A., Parsons A. R., Trott C. M., 2014a, *Phys. Rev. D*, 90, 023018
- , 2014b, *Phys. Rev. D*, 90, 023019
- Liu A., Tegmark M., 2011, *Phys. Rev. D*, 83, 103006
- Loeb A., Furlanetto S. R., 2013, *The First Galaxies in the Universe*. Princeton Univ. Press, Princeton, NJ
- Madau P., Meiksin A., Rees M. J., 1997, *ApJ*, 475, 429
- McGreer I. D., Mesinger A., D’Odorico V., 2015, *MNRAS*, 447, 499
- McQuinn M., 2012, *MNRAS*, 426, 1349
- McQuinn M., Lidz A., Zahn O., Dutta S., Hernquist L., Zaldarriaga M., 2007, *MNRAS*, 377, 1043
- McQuinn M., Oh S. P., Faucher-Giguère C.-A., 2011, *ApJ*, 743, 82
- Mesinger A., Ferrara A., Spiegel D. S., 2013, *MNRAS*, 431, 621
- Mesinger A., Furlanetto S., 2007, *ApJ*, 669, 663
- Mesinger A., Furlanetto S., Cen R., 2011, *MNRAS*, 411, 955
- Morales M. F., Wyithe J. S. B., 2010, *ARA&A*, 48, 127
- Pacucci F., Mesinger A., Mineo S., Ferrara A., 2014, *MNRAS*, 443, 678
- Parsons A. R., Liu A., Ali Z. S., Cheng C., 2015, preprint (arXiv:1503.05564)
- Parsons A. R., et al., 2010, *AJ*, 139, 1468
- , 2014, *ApJ*, 788, 106
- Planck Collaboration XIII, 2015, preprint (arXiv:1502.01589)
- Planck Collaboration XVI, 2014, *A&A*, 571, A16
- Pober J. C., et al., 2015, *ApJ*, 809, 62
- Press W. H., Schechter P., 1974, *ApJ*, 187, 425
- Pritchard J. R., Furlanetto S. R., 2007, *MNRAS*, 376, 1680
- Pritchard J. R., Loeb A., 2012, *Rep. on Prog. in Phys.*, 75, 086901
- Seager S., Sasselov D. D., Scott D., 1999, *ApJ*, 523, L1
- , 2000, *ApJS*, 128, 407
- Shaver P. A., Windhorst R. A., Madau P., de Bruyn A. G., 1999, *A&A*, 345, 380
- Sheth R. K., Tormen G., 1999, *MNRAS*, 308, 119
- Sobacchi E., Mesinger A., 2014, *MNRAS*, 440, 1662
- Springel V., Hernquist L., 2003, *MNRAS*, 339, 312
- Tingay S. J., et al., 2013, *PASA*, 30, 7
- Tozzi P., Madau P., Meiksin A., Rees M. J., 2000, *ApJ*, 528, 597
- Trott C. M., Wayth R. B., Tingay S. J., 2012, *ApJ*, 757, 101
- van Haarlem M. P., et al., 2013, *A&A*, 556, 2
- Wouthuysen S. A., 1952, *AJ*, 57, 31
- Yatawatta S., et al., 2013, *A&A*, 550, A136
- Zahn O., Mesinger A., McQuinn M., Trac H., Cen R., Hernquist L. E., 2011, *MNRAS*, 414, 727
- Zaroubi S., 2013, *The First Galaxies*, 396, 45
- Zel’dovich Y. B., 1970, *A&A*, 5, 84
- Zheng H., et al., 2014, *MNRAS*, 445, 1084